Curved Parametric Segments for the Stress Field of 3-D Dislocation Loops

Nasr M. Ghoniem
Mechanical and Aerospace Engineering Department, University of California at Los Angeles (UCLA), Los Angeles, CA 90095-1600
e-mail: ghoniem@ucla.edu

Under applied mechanical forces, strong mutual interaction or other thermodynamic forces, dislocation shapes become highly curved. We present here a new method for accurate computations of self and mutual interactions between dislocation loops. In this method, dislocation loops of arbitrary shapes are segmented with appropriate parametric equations representing the dislocation line vector. Field equations of infinitesimal linear elasticity are developed on the basis of isotropic elastic Green's tensor functions. The accuracy and computational speed of the method are illustrated by computing the stress field around a typical (110)–[111] slip loop in a BCC crystal. The method is shown to be highly accurate for close-range dislocation interactions without any loss of computational speed when compared to analytic evaluations of the stress field for short linear segments. Moreover, computations of self-forces and energies of curved segments are guaranteed to be accurate, because of the continuity of line curvature on the loop.

1 Introduction

Numerical simulations of plastic deformation with dislocation distributions are computationally very challenging, especially for engineering levels of strains, strain rates, and volumes. This particular aspect has been recognized in most Dislocation Dynamics (DD) simulations, either in 2-D (e.g., Ghoniem and Amodeo, 1988; Wang and LaSar, 1995), or in 3-D (e.g., DeVincre and Kubin 1994; Kubin et al., 1992; Ghoniem and Bacaloni, 1997; Zbib et al., 1998; Schwarz, 1997). Development of efficient yet accurate numerical techniques for DD simulations of plastic deformation is still in its infancy, especially in computationally intensive 3-D applications.

Dislocations in real crystals are generally curved because of their strong mutual interactions, externally applied stress fields, as well as thermodynamic forces resulting from gradients or changes in local chemical potentials. Moreover, extensive experimental evidence indicates that dislocation lines are generally curved, especially under the action of an externally applied stress, and at temperatures exceeding 0.2–0.3 of the material's melting point.

In some special cases, however, long straight dislocation segments are experimentally observed. This is particularly true in materials with high Peierel's potential barriers normal to specific crystallographic orientations (e.g., Si), or large mobility differences between screw and edge components (e.g., some BCC crystals at low temperature). It is apparent that very large curvature variations are expected, especially for strongly interacting dislocation loops. The accuracy of computing the dynamic shape of dislocation loops is thus dependent on how dislocation lines are discretized for field and force calculations.

In DD simulations of plastic deformation, the computational effort per time step is proportional to the square of the number of interacting segments, because of the long-range stress field associated with dislocation lines. It is therefore advantageous to reduce the number of interacting segments during such calculations. Recent 3-D calculations of dislocation interactions using straight segments are based on analytical solutions of the elastic field of either mixed segments, e.g., Zbib et al., 1998) and Schwarz and LeGoues (1997), or just screw and edge dislocation segments, e.g., DeVincre and Kubin (1994). Zbib et al. (1998) have shown that the length of each straight segment is roughly limited to the range of 50–200 units of Burgers vector. Longer segments may have substantial force variations, thus limiting the usefulness of one single equation of motion for the entire segment. Meanwhile, singular forces and stresses arise at sharp intersection points of straight segments, which result in divergence of the average force over the straight segment as the segment length is decreased. When the dislocation loop is discretized to either screw or edge components that move on a crystallographic lattice (Devincre and Kubin, 1994), the accuracy of strong dislocation interactions is compromised because line curvatures are crudely calculated. In addition, motion of dislocation segments on a fixed lattice produces inherent limitations to the accuracy of the overall dislocation dynamics. Schwartz (1998-I & II), on the other hand, has recently developed an adaptive method to reduce the segment size when dislocation interactions become strong. Using a modified form of the Brown formula (Brown, 1964) for the self-force on a segment, Schwarz circumvented the field divergence problem for very short segments. His work shows that substantial curvature and reconfiguration of interacting dislocations take place when one dislocation line closely approaches another one to form a junction, dipole, or other configurations. However, the number of straight segments required to capture these processes is very large, and the segment size may have to be on the order of a few Burgers vectors.

In this work, we develop a new and efficient computational method for calculations of the elastic field of arbitrary-shape, 3-D dislocation loops, in which the total field is the sum of constituent parameterized curved segments. A new procedure is presented where interconnected curved segments approximate the complex shape of a dislocation loop. Various conditions can be invoked on the shape functions that represent the loop, as desired by particular Dislocation Dynamics requirements. Since the shape of each segment is parameterized, a wide variety of representations can be used, in much the same way as the Finite Element Method (FEM) in continuum mechanics. Henceforth, we will term this method of computations simply the Finite Segment method (FSM), and will advance it for various types of parameterized curves, which will become important in specific applications. We present the differential geometry of

Contributed by the Materials Division for publication in the JOURNAL OF ENGINEERING MATERIALS AND TECHNOLOGY. Manuscript received by the Materials Division August 19, 1998; revised manuscript received November 8, 1998. Guest Editors: H. M. Zbib, J. P. Hirth, T. Khraishi, and R. Thomson.

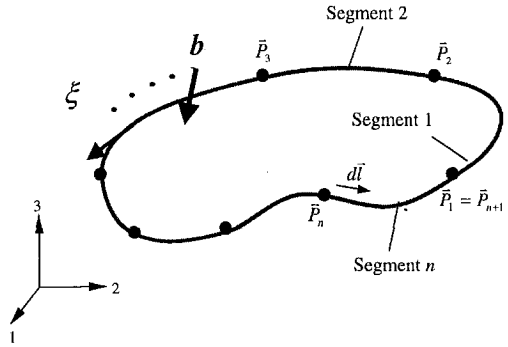

Fig. 1 Geometric representation of an arbitrary 3-D dislocation loop

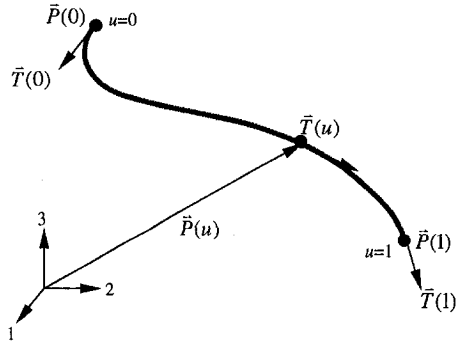

Fig. 3 Elements of a standard parametric curve

loops in Section 2, followed by a summary of the calculation procedure of the elastic field in Section 3. Several test cases for the accuracy and speed of our proposed method are then given in Section 4. Finally, conclusions and discussions are outlined in Section 5.

2 Computational Geometry of Dislocation Loops

2.1 Cubic Spline Parametric Segments. The core of an arbitrary-shape, 3-D dislocation loop can be represented as a continuous line, as shown in Fig. 1. Define the dislocation line vector, $\boldsymbol{\xi}$, as the tangent to the dislocation line. The Burgers vector **b** is prescribed as a displacement jump condition across any surface bounded by the dislocation line. Assume that the dislocation line is now segmented into (n_s) arbitrary curved segments, labeled ($1 \le i \le n_s$). Now consider only one segment, AB, as shown in Fig. 2.

We wish to compute field quantities (displacement vector, stress, and strain tensors) at point Q. For the parametric curve AB, the coordinates (x_i') of any point P on the line are represented by a set of parametric equations, as:

$$x_i' = a_{ij}u^j,$$

where the index i is for coordinate direction, and j for a polynomial power. The parameter u determines the coordinates of any point on the curve. For a cubic polynomial, both i and j are limited to 3. Summation is assumed over repeated indices. Generally, the coefficient matrix a_{ij} is 3×4. When the parameter u varies smoothly between 0 at A and 1 at B, another equivalent parametric form of the segment AB is given by:

$$\mathbf{P}(u) = \mathbf{r}' = F_1\mathbf{P}(0) + F_2\mathbf{P}(1) + F_3T(0) + F_4\mathbf{T}(1) \quad (1)$$

where:

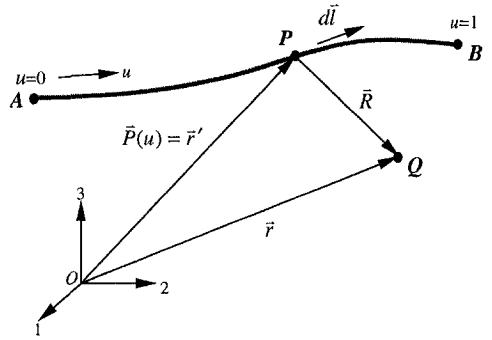

Fig. 2 Coordinates and notation for an isolated curved segment

$$F_1 = 2u^3 - 3u^2 + 1, \quad F_2 = -2u^3 + 3u^2,$$
$$F_3 = u^3 - 2u^2 + u, \quad F_4 = u^3 - u^2$$

are shape functions. Definitions of the position ($\mathbf{P}(0)$, $\mathbf{P}(1)$), and tangent ($\mathbf{T}(0)$, $\mathbf{T}(1)$) vectors at both ends are shown in Fig. 3. The tangent vector is obtained as:

$$\mathbf{T}(u) = \frac{\partial \mathbf{P}(u)}{\partial u}.$$

In component form, the position vector is given by:

$$x_i' = F_1P_i(0) + F_2P_i(1) + F_3T_i(0) + F_4T_i(1)$$

The arc length vector is given by:

$$d\bar{l} \equiv dx_i'\bar{e}_i \quad (i = 1, 2, 3)$$

where:

$$dx_i' = \{F_{1,u}P_i(0) + F_{2,u}P_i(1) + F_{3,u}T_i(0) + F_{4,u}T_i(1)\}du \quad (2)$$

and:

$$F_{1,u} = 6(u^2 - u), \quad F_{2,u} = -6(u^2 - u) = -F_{1,u},$$
$$F_{3,u} = 3u^3 - 4u + 1, \quad F_{4,u} = 3u^2 - 2u$$

Therefore, the radius vector $\bar{\mathbf{R}}$ is given by: $\bar{\mathbf{R}} \equiv X_i\mathbf{e}_i = \mathbf{r} - \mathbf{r}'$.

Once the parameter u is known, the entire differential geometry of the segment is determined. As will be shown next, the elastic field is only a function of this geometry. We will use the method of Green's tensor functions for an isotropic elastic medium to solve for the elastic field. It will be shown to be dependent on higher order derivatives of the radius vector $\bar{\mathbf{R}}$.

2.2 Other Parametric Forms. Under certain conditions, more convenient parametric forms can represent a dislocation loop. For example, a dislocation loop emitted from an isotropic Frank-Read source (i.e., all segments have the same mobility, regardless of their character) can be approximated as an ellipse or a planar circle. If additional thermodynamic forces exist in the material, such as a vacancy supersaturation driving force, the circular loop becomes a helix. Such circumstances are often observed in quenching or irradiation experiments. By properly choosing the coordinate system to be on the loop's glide plane, the following parametric representation may provide a good approximation for the case we discussed earlier.

$$x_1 = a\cos(\theta), \quad x_2 = b\sin(\theta), \quad x_3 = c\theta \quad (3)$$

where a, b, and c are constants. It is clear that proper selection of the constants can lead to circular, elliptic, or helical loop.

A continuous closed or open dislocation loop can be represented by a set of interconnected parametric curves. The exact

forms of these parametric curves depend on certain imposed geometric conditions on the loop. For example, if we demand curvature continuity, along with continuity of the first and second derivatives of of the position vector with respect to the parameter u, the tangent vector in Eq. (1) is completely determined. Thus the nodal positions on the loop will determine its shape. These details are not presented here, but will be given in future publications. Under some other conditions, as in most BCC crystals at low temperature, the expansion of the Frank-Read source is quite anisotropic, and edge-type segments have a much higher mobility as compared to screw-type segments. Long, nearly straight segments are often experimentally observed. A much simpler parametric representation is to use the general form of Eq. (1), with the following shape functions: $F_1 = 1 - u$, $F_2 = u$, $F_3 = F_4 = 0$. We will demonstrate the utility, numerical accuracy, and computational speed of each representation.

3 Isotropic Elastic Fields of Parametric Loops

3.1 Line Integral Representation of the Stress Field. Evaluation of the elastic field around an arbitrary-shape dislocation loop requires explicit development of the equations of elasticity for each finite segment. Since the stress components transform as second order tensors, the total stress field of the loop can be obtained by linear summation of the fields for individual segments. The procedure is quite lengthy, and is described in sufficient detail by Ghoniem and Bacaloni (1997) and Ghoniem (1999). In this paper, however, we highlight the main equations that are necessary to carry out stress field and interaction force computations. In this procedure, we first rewrite Burgers displacement equation for a loop in index tensor form. The displacement vector is then differentiated to obtain the elastic strain in an isotropic material as a line integral. The stress tensor is computed from the linear relationship between the strain and stress in an isotropic elastic material. The line integral for each stress component is finally discretized by parametric segments, and the total stress field computed by numerical quadrature integration over each segment. In the case of a planar circle, an ellipse or a helical loop, line integrals are computed with just one parametric equation. Summation of field contributions from loop segments is not required in these cases, since the entire loop is represented by one closed segment.

On any surface S', described by a set of points $\mathbf{r}'$, and which terminates at the dislocation line, the displacement vector components can be obtained as surface integrals of the derivatives of the Green's tensor functions U_{km}, in the following form:

$$u_m(\mathbf{r}) = b_i \int_{S'} C_{ijkl} U_{km,l}(\mathbf{r} - \mathbf{r}') dS'_j \tag{4}$$

where, for isotropic elastic materials, the elastic constants C_{ijkl} are given as:

$$C_{ijkl} = \lambda \delta_{ij}\delta_{kl} + G(\delta_{ik}\delta_{jl} + \delta_{il}\delta_{jk}) \tag{5}$$

and the Green's tensor functions are:

$$U_{km} = \frac{1}{8\pi G}\left[\delta_{km} R_{,pp} - \frac{\lambda + G}{\lambda + 2G} R_{,km}\right] \tag{6}$$

where λ and G are Lame's constants, δ_{ij} are the Kronecker delta functions, and $R_{,km}$ are successive derivatives of the radius vector $\mathbf{R}$. Differentiating the above expression with respect to j, we obtain:

$$U_{km,l} = \frac{1}{8\pi G}\left[\delta_{km} R_{,ppl} - \frac{\lambda + G}{\lambda + 2G} R_{,kml}\right] \tag{7}$$

From Eqs. (2)–(5), we derive a surface integral representation of the displacement vector components, u_m, as:

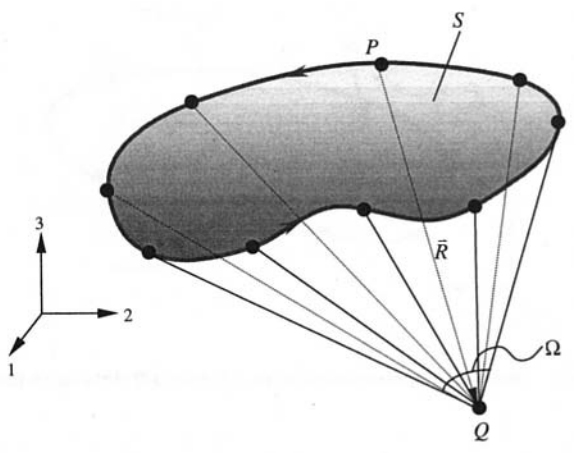

Fig. 4 Loop area (S) and solid angle Ω subtended by the loop

$$u_m(\bar{r}) = b_i \int_{S'} [\lambda \delta_{ij}\delta_{kl} + G(\delta_{ik}\delta_{jl} + \delta_{il}\delta_{jk})] \times \frac{1}{8\pi G}\left[\delta_{km} R_{,ppl} - \frac{\lambda + G}{\lambda + 2G} R_{,kml}\right] dS'_j \tag{8}$$

Equation (8) can be further developed, since the third order derivative of the radius vector represents a third order tensor of the form: $R_{,ppi} = -2X_i/|\mathbf{R}|^3$, and the solid angle subtended by the loop (see Fig. 4) is given by:

$$\Omega = \int_{S'} \frac{X_i\, dS_i}{|\mathbf{R}|^3} = -\frac{1}{2}\int_{S'} R_{,ppi} dS_i \tag{9}$$

Using Stokes theorem, together with Eq. (9), the surface integrals in the displacement equation can be readily converted to line integrals. The displacement vector components can now take the form:

$$u_i = -\frac{b_i \Omega}{4\pi} + \frac{1}{8\pi}\oint_C \left[\epsilon_{ikl} b_l R_{,pp} + \frac{m}{m-1}\epsilon_{kmn} b_n R_{,mi}\right] dl_k \tag{10}$$

In the infinitesimal deformation approximation, the linear strain-displacement relation is given by:

$$e_{ij} = \tfrac{1}{2}(u_{i,j} + u_{j,i}) \tag{11}$$

Now performing the derivatives, and inserting the result in Eq. (11), we obtain:

$$u_{i,j} = -\frac{b_i \Omega_{,j}}{4\pi} + \frac{1}{8\pi}\oint_C \left[\epsilon_{ikl} b_l R_{,ppj} + \frac{m}{m-1}\epsilon_{kmn} b_n R_{,mij}\right] dl_k \tag{12}$$

and:

$$e_{ij} = -\frac{b_i \Omega_{,j} + b_j \Omega_{,i}}{8\pi} + \frac{1}{8\pi}\oint_C \left[\frac{1}{2}(\epsilon_{jkl} b_l R_{,ppi} + \epsilon_{ikl} b_l R_{,ppj}) + \frac{m}{m-1}\epsilon_{kmn} b_n R_{,mij}\right] dl_k \tag{13}$$

It is shown by Ghoniem and Bacaloni (1997), and by Ghoniem (1999) that:

$$\Omega_{,j} = \tfrac{1}{2}\iint_S (R_{,ppll}dS_{j'} - R_{,pplj}dS_{l'}) = \tfrac{1}{2}\oint_C \epsilon_{jkl}R_{,ppl}dl_{k'} \quad (14)$$

which can be used to derive the strain components in line integral form, as follows.

$$e_{ij} = \frac{1}{8\pi}\oint_C \Big[-\frac{1}{2}(\epsilon_{jkl}b_i R_{,l} + \epsilon_{ikl}b_j R_{,l} - \epsilon_{ikl}b_l R_{,j} - \epsilon_{jkl}b_l R_{,i})_{,pp} + \frac{m}{m-1}\epsilon_{kmn}b_n R_{,mij}\Big] dl_{k'} \quad (15)$$

The dilatation is obtained by letting $i = r$ and $j = r$, thus:

$$e_{rr} = -\frac{1}{8\pi}\frac{m-2}{m-1}\oint_C \epsilon_{kmn}b_n R_{,mrr}dl_{k'} \quad (16)$$

when the linear stress-strain relationship is finally used in the form:

$$\sigma_{ij} = 2Ge_{ij} + \lambda e_{rr}\delta_{ij} \quad (17)$$

and Eqs. (15) and (16) are substituted into (17), we finally obtain the following compact line integral form for the stress components:

$$\sigma_{ij} = \frac{Gb_n}{4\pi}\oint_C \Big[\frac{1}{2}R_{,mpp}(\epsilon_{jmn}dl_{i'} + \epsilon_{imn}dl_{j'}) + \frac{m}{m-1}\epsilon_{kmn}(R_{,ijm} - \delta_{ij}R_{,ppm})dl_{k'}\Big] \quad (18)$$

Several equivalent forms of the line integral representations are available in the literature (see, for example, Hirth and Lothe, 1982) for a compact vector representation, or deWit (1960) for formal procedures. However, the intent in this section is to describe a new computational procedure in sufficient detail to allow for actual numerical calculations, rather than formal theoretical developments, as will be shown next.

3.2 Explicit Forms for the Stress Field of a Parametric Segment. The closed-loop line integral for the total stress field of a dislocation loop will now be written as a sum of open line integrals for individual segments, as:

$$\sigma_{ij} = \int_A^B \{..\} + \int_B^C \{..\} + \ldots . \quad (19)$$

For just one segment, such as AB, the line integral is found to contain only four functions of the following form:

$$\sigma_{ij} = \frac{G}{8\pi}\int_A^B [g_1 + g_2 + g_3 + g_4]du \quad (20)$$

where:

$$g_1 = b_n R_{,mpp}\epsilon_{jmn}(dl_i'/du) = b_n R_{,mpp}\epsilon_{jmn}x'_{i,u}$$

$$g_2 = b_n P_{,mpp}\epsilon_{imn}(dl_j'/du) = b_n R_{,mpp}\epsilon_{imn}x'_{j,u}$$

$$g_3 = \frac{2}{1-\nu}b_n R_{,mij}\epsilon_{kmn}(dl_k'/du) = \frac{2}{1-\nu}b_n R_{,mij}\epsilon_{kmn}x'_{k,u}$$

$$g_4 = -\frac{2}{1-\nu}b_n\delta_{ij}R_{,mpp}\epsilon_{kmn}(dl_k'/du) = -\frac{2}{1-\nu}b_n\delta_{ij}R_{,mpp}\epsilon_{kmn}x'_{k,u}du \quad (21)$$

Ghoniem and Bacaloni (1997), and Ghoniem (1999) developed explicit forms for the stress field components in detail. An example of just one component is given below:

$$\sigma_{11} = \frac{G}{8\pi}\int_A^B \Bigg\{ \Big[b_2\Big(-2R_{,113} + \frac{2\nu}{1-\nu}(R_{,223} + R_{,333})\Big) + b_3\Big(2R_{,112} - \frac{2\nu}{1-\nu}(R_{,222} + R_{,332})\Big)\Big] x'_{1,u} + \Big[-b_1\frac{2}{1-\nu}(R_{,223} + R_{,333}) + b_3\frac{2}{1-\nu}(R_{,221} + R_{,331})\Big] x'_{2,u} + \Big[+b_1\frac{2}{1-\nu}(R_{,222} + R_{,332}) - b_2\frac{2}{1-\nu}(R_{,221} + R_{,331})\Big] x'_{3,u} \Bigg\} du \quad (22)$$

The integral arguments, $R_{,113}$, $R_{,223}$, etc. represent successive derivatives of the radius vector with respect to the coordinate system 1, 2, 3. Details of this procedure, as well as explicit forms of parametric integrals similar to Eq. (22), are all given elsewhere (Ghoniem (1999)) and will not be repeated here.

4 Computational Accuracy and Speed

One of the objectives of determining the stress field around dislocation loops is to calculate the associated Peach-Koehler force on neighboring loops (interaction force), or on themselves as they change shape (self-force). To assess the influence of various discretization methods on the accuracy of the stress fields, and hence on the P-K force itself, we present here results of calculations for a representative example of an isolated slip-type loop.

Consider a typical slip loop in a BCC crystal, and assume that the loop is perfectly circular on the (110) slip plane. The Burgers vector is directed along the [111]-direction. The loop's radius is 200 b, where b is the magnitude of the Burgers vector. All length scales are measured in units of b, and all stress magnitudes are in units of the shear modulus, G. To demonstrate the accuracy and computational speed of various loop segmentation techniques, we choose to discuss the distribution of only one stress component. The following results are for the shear stress, σ_{12}, referred to the (110)-slip plane, where the 1-axis is [010]-direction and the 3-axis is the [110]-direction.

Figure 5 shows the shear stress distribution in the vicinity of the (110)–[111] slip loop, calculated for a number of linear segments (n_s) of 4, 10, 200 and 1000, respectively. The order of Gaussian quadrature integration is denoted by (q) on the figure. Calculations with an increasing number of linear seg-

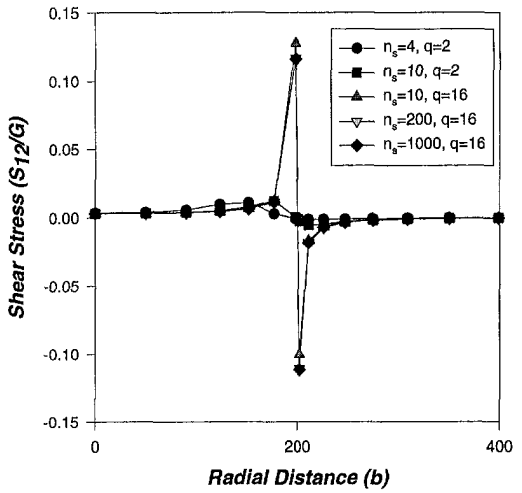

Fig. 5 Influence of the number of straight segments (n_s) and quadrature order (q) on the shear stress distribution around a (110) - [111] slip loop

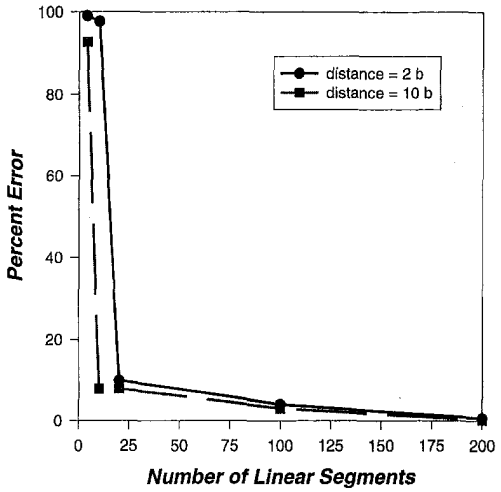

Fig. 6 Converged field error as a function of the number of straight linear segments, at two different distances from the dislocation loop edge

ments show that the stress field is convergent with the number segments (n_s). It is interesting to note that while the shear stress is singular exactly at the dislocation core, a consequence of the displacement jump condition, it is not entirely symmetric with respect to the radial distance away from the core. The value of the stress field changes from positive to negative as we cross the dislocation core, and is finite at the center of the loop (see table (1) for exact numerical values showing the asymmetry). Obviously, since the field decays to zero at infinity, the field asymmetry is thus dependent on the loop radius (or curvature). This observation may seem to be a subtle point, but it will be shown to be quite important to the accurate determination of the self-force on curved loop segments.

It is clear that as the number of discrete linear segments is increased, the accuracy of the stress field in close proximity of the loop edge is improved. It is noted that field accuracy is determined not only by the total number of linear segments, but also by the order of the numerical quadrature employed. The closest points to the loop edge are 1.5 b away.

Figure 6 summarizes the dependence of the shear stress error on the number of linear segments at distances of 2 b and 10 b from the dislocation core. The stress field value converges for all $n_s \geq 200$, to within six significant digits. This converged value is used as a reference for these calculations. Moreover, additional computations have also been performed using analytical forms for straight linear segments given by Hirth and Lothe (1982). Remarkable agreement with numerical quadrature integration is obtained. Nevertheless, required stress transformations from the local segment coordinates to the global coordinates renders the analytical expressions less efficient as the number of segments is increased. When equivalent analytical solutions for the stress field of straight segments in the global coordinate system are used (see DeVincre and Condat, 1992 and Schwarz, 1997), this problem is alleviated.

Geometric representation of complex shape dislocation loops via spline segments is inherently accurate, because curved splines can be adjusted to approximate the dislocation line to any desired accuracy. Since all elastic field quantities are just functions of the radius vector and its higher order derivatives, field errors are expected to be proportional to the ratio of spline deviation from the actual geometry to the magnitude of the radius vector. Partial cancellation of these errors may also be achieved as a result of the summation nature of line integrals. On an intuitive basis, one expects that good field accuracy is achievable with a relatively small number of spline segments. To illustrate this point further, we show in Fig. 7 the influence of increasing the number of spline segments on the accuracy of the shear stress for the same slip loop. In these calculations, we fix the order of numerical quadrature to 16. It is obvious that very small improvements at distances of 1.5 b or less from the loop edge are obtained when the circle is represented by more than three to four spline segments. The effect of the order of numerical quadrature is made clear in Fig. 8, where the number of curved spline segments is fixed to only three. At close distances from the dislocation core, a low order quadrature integration scheme tends to "smear out" the asymptotic singular nature of the field. Therefore, very good accuracy in field and force calculations can be obtained with 3–4 spline segments combined with a numerical quadrature order of 16.

It may be desirable to represent a complex shape planar dislocation loop by a perfect circle, and obtain the elastic field quantities using numerical integration. In such a case, very rapid calculations can be performed, if the entire loop is represented by just one parametric equation of a full circle (e.g., Eq. (3), with $a = b$ = radius, and $c = 0$). This situation is envisioned for calculations of the P-K force resulting from small irregular planar loops at distances from their center larger than the loop diameter. No segmentation would be required in this case. Figure 9 shows the distribution of the stress field around our example slip loop, utilizing various quadrature orders with a single parametric equation. Spline field distribution is compared to

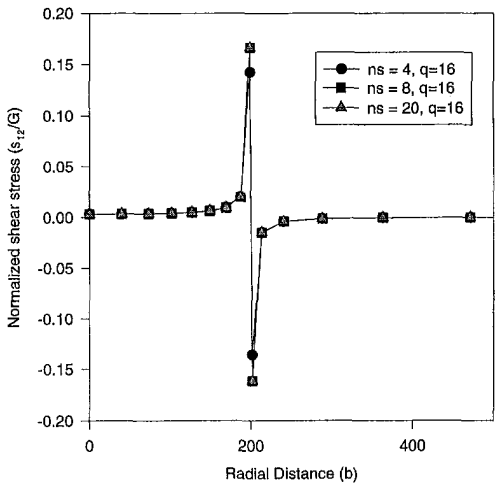

Fig. 7 Effects of number of curved spline segments on the accuracy of the shear stress around a (110) - [111] slip loop

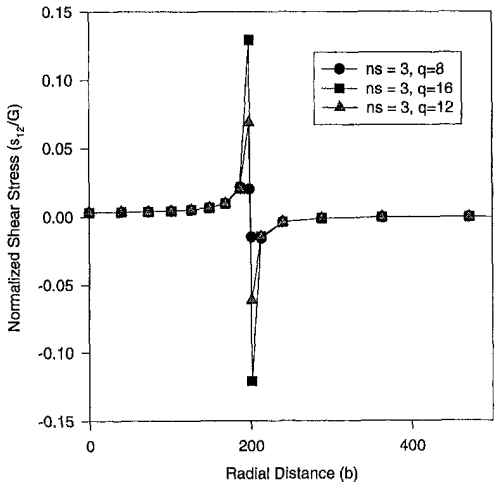

Fig. 8 Effects of Gaussian quadrature order on field accuracy for (110) – [111] slip loop

calculations with 2000 linear segments. It is shown that while the accuracy of field (hence force) calculations is poor within distances less than 10 b from the dislocation core, the results are quite good for all space, excluding these short distances. Thus, such approximation can be effectively used for far field calculations (say at distances greater than $\frac{1}{20}$ of the loop radius from the loop edge). If shape deviations from the circle are quite small, then such an approximation can be powerful for far-field calculations of small, nearly circular loops. Similar arguments can be made for helical loops, which result from vacancy supersaturation in quenched or irradiated materials.

To appreciate the absolute accuracy of the various numerical integration and analytic solution methods utilized in the present work, numerical values of the normalized shear stress distributions are shown in Table 1 below. The results at close distances (1.5 b and 13.5 b) are especially highlighted.

5 Discussion and Conclusions

Although the elements of dislocation theory have been almost completely developed over the past several decades, the lack of efficient computational methods for the interaction and motion of *dislocation ensembles* has just been recently advanced. However, significant difficulties are now encountered in the simulation of 3-D Dislocation Dynamics because of complex topological configurations on the one hand, and the long-range internal force field on the other. The present method is aimed at the development of an efficient computational scheme for evaluation of internal Peach-Koehler forces and interaction energies amongst complex dislocation configurations. This is achieved by dividing dislocation loops into a small number of curved segments, which if appropriately chosen, can represent the dislocation core to great accuracy. Studying a particular example of a typical slip loop in BCC crystals has shown the usefulness of the present method, but the procedure is rather general.

Representation of dislocation loops by parametric equations, coupled with a fast integration technique for field variables as line integrals, appear to have a number of potential advantages. These are summarized as:

(1) A complex dislocation loop (e.g., during the operation of a Frank-Read source, or during the process of cross-slip for nonplanar loops) can be represented by a relatively few number of curved segments. The Peach-Koehler force resulting from the interaction of one loop with another can thus be numerically computed as a fast summation over those few curved segments. This can be quite advantageous in 3-D Dislocation Dynamics, because the force computation is proportional to the square of the number of segments. Thus a reduction of two orders of magnitude in the number of segments will result in four order of magnitude reduction in force calculations.

(2) Because of the high accuracy of curvature representation in the present method, the computation of self-forces and self-energies of individual segments within one loop is inherently accurate.

(3) When the P-K force and other elastic field quantities are required at distances greater than approximately $\frac{1}{20}$ – $\frac{1}{10}$ of a loop diameter from its core, very useful approximations of the loop can be advantageously used within the current line integral context. Thus, planar circles can readily approximate the core of small irregular loops, while dipolar loops can be treated as elongated ellipse, etc.

(4) Although two nodes bound each segment, the dislocation core is described by a continuous curve in-between. Thus, the segment has an infinite number of degrees of freedom. This particular aspect can be quite significant in a variational development of the equations of motion (see Ghoniem, 1999). Other formulations of the equations of motion of straight segments use an averaging scheme for force variations on the segment. Thus, when the segment is long, averaging of the P-K force at a central nodal position becomes less accurate.

(5) Since the dislocation loop is continuously described by a set of curves, updating the loop shape in dislocation Dynamics can utilize the existence of such "shape functions." The need to artificially impose connectivity conditions where the straight pieces do not fit with one another upon updating the positions of their central nodes is thus alleviated.

The in-plane self-force at a point on the a planar loop has been shown by Gavazza and Barnett (1976) to be given by:

$$\mathbf{f.m} = -\kappa E(\tau) + \tfrac{1}{2} b_i n_j \{\sigma_{ij}(P + \epsilon\mathbf{m}) + \sigma_{ij}(P - \epsilon\mathbf{m})\} \quad (23)$$

where the local unit tangent, principal normal and curvature are $\mathbf{t}$, $\mathbf{m}$, and κ, respectively. $E(\mathbf{t})$ is a prelogarithmic energy factor for an infinitely long dislocation line. The distance ϵ represents a position very close to the core (e.g., 1.5 b in Table 1). Barnett (1980) generalized Eq. (23) to noncircular loops, and showed that in the limit, the force averaging given by the last two terms can be computed in terms of the loop curvature at the point P. Thus, the asymptotic form of the local self-force is given by:

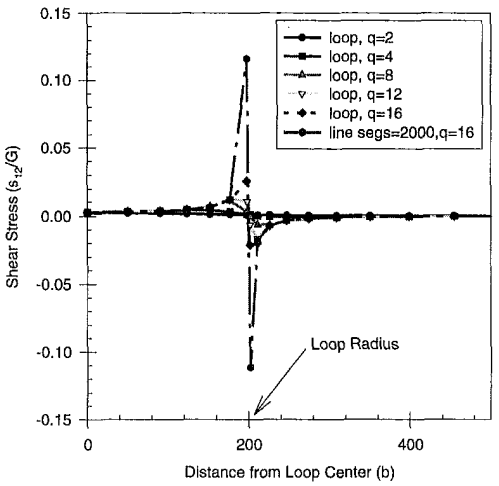

Fig. 9 Influence of numerical quadrature integration order on stress field accuracy for a slip loop represented by a single circular parametric equation

Table 1 Normalized shear stress distribution calculated with different parametric and analytic forms

Position (b)	Single Loop	Cubic Spline		Straight Segments							
				Analytic	Numerical q=3	Analytic	Numerical q=3	Analytic	Numerical q=3	Analytic	Numerical q=3
	Ns =1	Ns=3	Ns=10	Ns=4		Ns=10		Ns=100		Ns=1000	
0.0000	3.0357e-3	3.2684e-3	3.0364e-3	3.8652e-3	3.9299e-3	3.1397e-3	3.1399e-3	3.0367e-3	3.0367e-3	3.0357e-3	3.0357e-3
40.0000	3.1388e-3	3.3620e-3	3.1396e-3	4.0453e-3	4.0800e-3	3.2541e-3	3.2543e-3	3.1399e-3	3.1399e-3	3.1388e-3	3.1388e-3
73.3000	3.4185e-3	3.6591e-3	3.4196e-3	4.5371e-3	4.3257e-3	3.5679e-3	3.5680e-3	3.4199e-3	3.4199e-3	3.4185e-3	3.4185e-3
101.9000	3.8951e-3	4.1676e-3	3.8966e-3	5.3831e-3	4.7645e-3	4.1116e-3	4.1088e-3	3.8972e-3	3.8972e-3	3.8952e-3	3.8952e-3
126.9000	4.6757e-3	4.9934e-3	4.6778e-3	6.7836e-3	6.5662e-3	5.0193e-3	4.9934e-3	4.6789e-3	4.6789e-3	4.6757e-3	4.6757e-3
149.1000	6.0544e-3	6.4347e-3	6.0574e-3	9.2869e-3	0.0127	6.6516e-3	6.5981e-3	6.0602e-3	6.0602e-3	6.0539e-3	6.0539e-3
169.1000	8.9764e-3	9.4873e-3	9.0170e-3	0.0147	0.0226	0.0102	0.0110	9.0276e-3	9.0276e-3	9.0112e-3	9.0112e-3
187.3000	0.0211	0.0204	0.0197	0.0347	5.4045e-3	0.0233	0.0233	0.0198	0.0198	0.0197	0.0197
198.5000	0.0206	0.1291	0.1627	0.2890	-1.9946e-3	0.1902	1.1502e-3	0.1564	0.1510	0.1539	0.1539
201.5000	-0.0167	-0.1209	-0.1582	-0.0755	-2.6655e-3	-0.1194	-6.5012e-3	-0.1468	-0.1384	-0.1492	-0.1492
213.5000	-0.0163	-0.0145	-0.0151	-7.8487e-3	-3.1538e-3	-0.0125	-0.0102	-0.0150	-0.0150	-0.0151	-0.0151
240.5000	-4.1846e-3	-3.8641e-3	-4.2006e-3	-2.2677e-3	-1.9071e-3	-3.6091e-3	-3.6679e-3	-4.1956e-3	-4.1956e-3	-4.2044e-3	-4.2044e-3
288.5000	-1.4573e-3	-1.2947e-3	-1.4557e-3	-8.2006e-4	-8.0531e-4	-1.2972e-3	-1.2984e-3	-1.4551e-3	-1.4551e-3	-1.4569e-3	-1.4569e-3
363.5000	-5.4672e-4	-4.7702e-4	-5.4637e-4	-3.2030e-4	-3.2019e-4	-4.9849e-4	-4.9848e-4	-5.4622e-4	-5.4622e-4	-5.4673e-4	-5.4673e-4
471.5000	-2.1421e-4	-1.8559e-4	-2.1409e-4	-1.2944e-4	-1.2947e-4	-1.9775e-4	-1.9775e-4	-2.1404e-4	-2.1404e-4	-2.1421e-4	-2.1421e-4
618.5000	-8.7221e-5	-7.5457e-5	-8.7175e-5	-5.3808e-5	-5.3813e-5	-8.1019e-5	-8.1019e-5	-8.7157e-5	-8.7157e-5	-8.7221e-5	-8.7221e-5
810.5000	-3.7034e-5	-3.2053e-5	-3.7016e-5	-2.3140e-5	-2.3140e-5	-3.4509e-5	-3.4509e-5	-3.7008e-5	-3.7008e-5	-3.7034e-5	-3.7034e-5

$$\mathbf{f.m} = -\kappa E(\mathbf{t}) + \kappa\{E(\mathbf{t}) + E''(\mathbf{t})\} \ln \frac{8}{\kappa\epsilon} \qquad (24)$$

where E'' is the second derivative of the prelogarithmic term. It is interesting to note that once the local curvature, κ, and the core size, ϵ, are both given, the self-force is accurately determined at any point on the loop. The total Peach-Koehler force at a point is composed of the self-force given by Eq. (24) and contributions from other segments on the loop. Schwarz (1998 I & II) evaluated contributions of various terms to the P-K force given by Eq. (24). He showed that the contributions from the last two terms are completely dominant, especially for loops with $\kappa < 0.1$ nm^{-1}. Nonlocal contributions to the force have also been shown to be small. The segment size (i.e., the change from local to nonlocal force contributions) is only significant when substantial variations in the dislocation curvature along this particular segment are encountered. Thus, when one uses a straight dislocation segment, its size must be very small so as to enhance the non-local contributions (i.e., from neighboring segments). This is again difficult because the force distribution along one segment diverges as the segment gets smaller because of singularities at the sharp corners of a straight segment.

Since the current procedure is purely numerical, an interesting question poses itself. With the potential advantages of the present method, does it suffer from being computationally slow compared to implementation of analytical solutions for short straight segments? To answer this question, a number of computational speed tests have been performed on a DeC-alpha workstation (433 MHz). The results are given in Table 2. While numerical calculations with a fourth order quadrature are slightly slower than corresponding analytical solutions, they are indeed faster for a second order quadrature integration scheme.

Table 2 Comparison of the computational speed for stress field calculations for parametric and analytic forms

1000 Linear Segments		
Analytic	Numerical, q = 2	Numerical, q = 4
360	347	515

Same Accuracy Test		
Analytic	Analytic	Numerical
100 Segments	1000 Segments	Cubic Spline, 3 Segments, q=16
88	360	66

- *milli-seconds on DeC Alpha 433 MHz*

These comparisons are given for a loop divided into straight linear segments. What is also remarkable is the fact that numerical integration with only three cubic spline segments are much faster than corresponding analytical solutions using 100 (or 1000) straight segments to achieve the same numerical accuracy. The main reasons for these results are:

(1) The numerical calculations are nothing more than fast summations performed over terms containing various combinations of the components of the vector distance between the point and the loop line vector.

(2) The analytical expressions are obtained in the frame of reference of a straight segment. Thus, coordinate transformations to a global system result in additional computational overhead, which increases with the number of segments. As mentioned before, the form utilized by DeVincre and Condat (1992) in the global system alleviates this problem.

Acknowledgments

The author would like to acknowledge the financial support of Lawrence Livermore National Laboratory (LLNL) through the Materials Research Institute (MRI) and the ASCI Computing initiative with the Chemistry and Materials Science Directorate (CMS). Discussions with Drs. Tomas de la Rubia and David Lassila have been helpful to the development of the current method, while the assistance of Marco Bacaloni with tensor algebra during the initial formulation period is acknowledged. Critical reading of the manuscript prior to publication by Professor A. Mal (UCLA) is also acknowledged.

References

D. Barnett, 1980, *Dislocation Modeling of Physical Systems,* A. Ashby et al., eds., Pergamon Press, 224.

L.M. Brown, 1964, *Philos. Mag.,* 10, 441.

R. deWit, 1960, *Sol. State Phys.,* 10, 269.

B. DeVincre and M. Condat, 1992, *Acta Metall. Mater.,* 40, 2629.

B. DeVincre and L.P. Kubin, 1994, *Model. Simul. Mater. Sci. Eng.,* 2, 559.

S.D. Gavazza and D.M. Barnett, 1976, *J. Mech. Phys. Solids,* 24, 171.

N.M. Ghoniem and R. Amodeo, 1998, "Computer Simulation of Dislocation Pattern Formation," *Solid State Phenomena,* 3 and 4, 377.

N.M. Ghoniem and M. Bacaloni, 1997, Eng. Rept., UCLA/MATMOD-97-01, Department of Mechanical and Aerospace Eng., UCLA, Los Angeles, CA.

N.M. Ghoniem, 1999, to be published.

J.P. Hirth and J. Lothe, 1982, *Theory of Dislocations,* 2nd Ed., Wiley, New York.

L.P. Kubin, G. Canova, M. Condat, B. DeVincre, V. Pontikis, and Y. Brechet, 1992, *Sol. State Phenomena,* 23–24, 445.

K.W. Schwarz, 1997, *Phys. Rev. Lett.,* 78, 4785.

K.W. Schwarz and LeGoues, 1997, *Phys. Rev. Lett.,* 79, 1877.

K.W. Schwarz, 1998, "Simulation of dislocations on the Mesoscopic Scale," Parts I and II, to be published.

H.Y. Wang and R. LeSar, 1998, *Philos. Mag.,* A71, 149.

H.M. Zbib, M. Rhee, and J.P. Hirth, 1998, *Int. J. Mech. Sci.,* 40, 113.